

You might find this additional information useful...

This article cites 47 articles, 16 of which you can access free at:

<http://ajpheart.physiology.org/cgi/content/full/274/5/H1715#BIBL>

This article has been cited by 13 other HighWire hosted articles, the first 5 are:

Theoretical model of blood flow autoregulation: roles of myogenic, shear-dependent, and metabolic responses

B. E. Carlson, J. C. Arciero and T. W. Secomb
Am J Physiol Heart Circ Physiol, October 1, 2008; 295 (4): H1572-H1579.
[\[Abstract\]](#) [\[Full Text\]](#) [\[PDF\]](#)

Development and Validation of an Integrated Computational Model of Cerebral Blood Flow and Oxygenation

I. K. Moppett and J. G. Hardman
Anesth. Analg., October 1, 2007; 105 (4): 1094-1103.
[\[Abstract\]](#) [\[Full Text\]](#) [\[PDF\]](#)

Cerebral blood flow velocity during mental activation: interpretation with different models of the passive pressure-velocity relationship

R. B. Panerai, M. Moody, P. J. Eames and J. F. Potter
J Appl Physiol, December 1, 2005; 99 (6): 2352-2362.
[\[Abstract\]](#) [\[Full Text\]](#) [\[PDF\]](#)

Phase dynamics in cerebral autoregulation

M. Latka, M. Turalska, M. Glaubic-Latka, W. Kolodziej, D. Latka and B. J. West
Am J Physiol Heart Circ Physiol, November 1, 2005; 289 (5): H2272-H2279.
[\[Abstract\]](#) [\[Full Text\]](#) [\[PDF\]](#)

Blood pressure and blood flow variation during postural change from sitting to standing: model development and validation

M. S. Olufsen, J. T. Ottesen, H. T. Tran, L. M. Ellwein, L. A. Lipsitz and V. Novak
J Appl Physiol, October 1, 2005; 99 (4): 1523-1537.
[\[Abstract\]](#) [\[Full Text\]](#) [\[PDF\]](#)

Medline items on this article's topics can be found at <http://highwire.stanford.edu/lists/artbytopic.dtl> on the following topics:

Physiology .. Hemodynamics
Physiology .. Cerebrovascular Circulation
Physiology .. Blood Circulation
Physiology .. Arterial Circulation
Physiology .. Blood Pressure
Computer Science .. Mathematical Modeling

Updated information and services including high-resolution figures, can be found at:

<http://ajpheart.physiology.org/cgi/content/full/274/5/H1715>

Additional material and information about *AJP - Heart and Circulatory Physiology* can be found at:

<http://www.the-aps.org/publications/ajpheart>

This information is current as of November 25, 2009 .

Interaction among autoregulation, CO₂ reactivity, and intracranial pressure: a mathematical model

MAURO URSINO AND CARLO ALBERTO LODI

Department of Electronics, Computer Science and Systems, University of Bologna, I-40136 Bologna, Italy

Ursino, Mauro, and Carlo Alberto Lodi. Interaction among autoregulation, CO₂ reactivity, and intracranial pressure: a mathematical model. *Am. J. Physiol.* 274 (*Heart Circ. Physiol.* 43): H1715–H1728, 1998.—The relationships among cerebral blood flow, cerebral blood volume, intracranial pressure (ICP), and the action of cerebrovascular regulatory mechanisms (autoregulation and CO₂ reactivity) were investigated by means of a mathematical model. The model incorporates the cerebrospinal fluid (CSF) circulation, the intracranial pressure-volume relationship, and cerebral hemodynamics. The latter is based on the following main assumptions: the middle cerebral arteries behave passively following transmural pressure changes; the pial arterial circulation includes two segments (large and small pial arteries) subject to different autoregulation mechanisms; and the venous cerebrovascular bed behaves as a Starling resistor. A new aspect of the model exists in the description of CO₂ reactivity in the pial arterial circulation and in the analysis of its nonlinear interaction with autoregulation. Simulation results, obtained at constant ICP using various combinations of mean arterial pressure and CO₂ pressure, substantially support data on cerebral blood flow and velocity reported in the physiological literature concerning both the separate effects of CO₂ and autoregulation and their nonlinear interaction. Simulations performed in dynamic conditions with varying ICP underline the existence of a significant correlation between ICP dynamics and cerebral hemodynamics in response to CO₂ changes. This correlation may significantly increase in pathological subjects with poor intracranial compliance and reduced CSF outflow. In perspective, the model can be used to study ICP and blood velocity time patterns in neurosurgical patients in order to gain a deeper insight into the pathophysiological mechanisms leading to intracranial hypertension and secondary brain damage.

intracranial hemodynamics; cerebral blood flow; cerebral blood volume; cerebrovascular control mechanisms

THE CEREBROVASCULAR BED in humans and animals is subjected to the action of sophisticated regulatory mechanisms that work to maintain an adequate cerebral blood flow (CBF) for functional and metabolic needs. Intracranial vessels respond promptly to changes in cerebral perfusion pressure (CPP; cerebral arterial pressure minus cerebral venous pressure); the response, called autoregulation, ensures that CBF remains approximately constant in the CPP range of 50–150 mmHg (38). Moreover, cerebral vasculature is particularly sensitive to chemical stimuli, especially O₂ and CO₂ tension in arterial blood. These mechanisms interact in complex nonlinear ways in response to perturbations affecting pressure and blood concentration levels simultaneously.

There are many factors that make the analysis of cerebrovascular regulation particularly complicated.

First, consecutive vascular segments in the brain contribute differently to CBF control, a phenomenon often referred to as “segmental heterogeneity” (6). Some authors have observed that the large pial vessels play a major role in the regulatory response to moderate arterial pressure changes, whereas small pial arteries undergo massive vasodilation when CPP approaches the lower autoregulation limit (25, 29).

In addition, cerebral circulation takes place within a closed space (the skull and the craniospinal axis) with only a limited capacity to buffer blood volume changes; consequently, any modification in vessel caliber (either passive or induced by cerebrovascular regulatory mechanisms) may affect intracranial pressure (ICP) through changes in cerebral blood volume (CBV). Because ICP is the extravascular pressure of cerebral vessels and is almost equal to pressure in the large cerebral veins, its changes can have a significant impact on cerebral hemodynamics.

Because of the close relationship among the action of cerebrovascular control mechanisms, CBV, and ICP, CBF can be affected by several noncirculatory aspects of intracranial dynamics, especially craniospinal elasticity (defined by the intracranial pressure-volume relationship) and the circulation of cerebrospinal fluid (CSF).

The interaction among ICP, CBV, and cerebrovascular regulation must be taken into account in the treatment of patients with severe brain lesions. Changes in arterial CO₂ pressure (Pa_{CO₂}) and mean systemic arterial pressure (SAP) are frequently used in neurosurgical intensive care units to assess the status of cerebrovascular control mechanisms (8, 48). Moreover, manipulation of arterial CO₂ concentration is routinely used as a therapeutic means in controlling ICP and adjusting CBF to metabolic requirements (34, 37). However, uncontrolled changes in CO₂ or in arterial pressure can have a dramatic impact on ICP and CBF, leading to acute intracranial hypertension and cerebral ischemia (12).

The complexity of the aforementioned relationships makes it difficult to achieve a clear understanding of cerebrovascular control in simple qualitative terms. For this reason, various mathematical models of cerebral hemodynamics and ICP dynamics have been presented in past years (7, 21, 22, 31, 47, 49). We recently developed a mathematical model of the interaction among cerebral autoregulation, CBV changes, and ICP in humans (50, 51). The model was able to reproduce various phenomena concerning ICP, such as the genesis of plateau waves (51), the ICP response to arterial pressure perturbations (14), or the ICP changes in-

duced by bolus injection within the craniospinal space (PVI tests) (52).

The aim of this study was to significantly improve and extend the previous model to include the CO₂ reactivity of cerebral vessels, its nonlinear interaction with ICP and with cerebral autoregulation, and the description of the transcranial Doppler (TCD) velocity signal. The TCD technique, in fact, is routinely used today to assess cerebral hemodynamics due to its characteristics of noninvasiveness and continuous data acquisition (1).

There are two main justifications for developing this new model. We aimed to 1) demonstrate that several experimental results on cerebral autoregulation and chemical CBF regulation presented in past years can be summarized into a single theoretical setting, and 2) improve the interpretation of clinical maneuvers concerning cerebrovascular control and ICP dynamics.

The present preliminary study presents the model, its justification on the basis of current physiological knowledge, and its validation through experimental results taken from physiological literature. A second, related study (27) presents a sensitivity analysis of model parameters and validation of the model on the basis of clinical data from real patients with severe head trauma.

QUALITATIVE MODEL DESCRIPTION

The model is qualitatively presented, with attention focused on its new aspects. A more thorough analysis can be found in previous reports (50, 51). The complete set of mathematical equations is given in the APPENDIX.

Intracranial Hemodynamics and CSF Dynamics

The main biomechanical law at the basis of intracranial dynamics is the constancy of the overall volume contained in the craniospinal space. This principle, known as the Monro-Kellie doctrine, implies that any volume variation in an intracranial compartment causes a compression or dislocation of the remaining volumes, accompanied by an alteration in ICP. This phenomenon is mathematically reproduced by means of intracranial compliance (C_{ic}), which represents the capacity of the craniospinal system to store a volume load. We assumed that this quantity is inversely proportional to intracranial pressure (P_{ic}) through a constant parameter called the elastance coefficient (k_E) (5, 31)

$$C_{ic} = \frac{1}{k_E \cdot P_{ic}}$$

In the present model, volume changes in the intracranial cavity are ascribed to four compartments: large pial artery volume (V_1), small pial artery volume (V_2), cerebral venous volume (V_v), and CSF volume (V_{CSF}). The following volume preservation equation holds

$$C_{ic} \left(\frac{dP_{ic}}{dt} \right) = \frac{1}{k_E \cdot P_{ic}} \left(\frac{dP_{ic}}{dt} \right) = \frac{dV_1}{dt} + \frac{dV_2}{dt} + \frac{dV_v}{dt} + \frac{dV_{CSF}}{dt}$$

where t is time.

The electric analog in Fig. 1 represents the four intracranial compartments considered in the model and their mutual relationships, together with the extracranial venous drainage pathway. These are briefly described in the following sections.

Pial arteries and arterioles. Pial arteries and arterioles comprise the sections of the cerebrovascular bed directly under the control of regulatory mechanisms. We make a distinction between two consecutive segments, the large pial arteries (proximal segment) and the medium and small pial arteries (distal segment). In the following equation, subscript $j = 1$ indicates a quantity or a parameter that belongs to the proximal arteries, whereas subscript $j = 2$ refers to the distal arterioles. Each segment is represented by a transverse hydraulic capacity (C_j), at which all blood volume changes are concentrated, and a longitudinal hydraulic conductance (G_j), which reproduces the pressure drop upstream and downstream of the capacity. The distinction between two segments is justified by the heterogeneity of cerebrovascular regulation (6).

Conductance and blood volume changes are calculated by simulating each segment as the parallel arrangement of several vessels with equal radius. Blood volumes are proportional to the second power of the inner radius, whereas conductances are proportional to the fourth power of the inner radius, according to the Hagen-Poiseuille law (33). This representation does not aim at reproducing the actual anatomic configuration of the cerebrovascular bed; rather, it aims only to describe how a certain variation of vessel caliber, induced by cerebral autoregulation and/or CO₂ reactivity, can influence vascular resistance and blood volume in a given segment.

A value for the inner radius (r_j) is computed starting from the equilibrium of forces acting on the wall of the vessel, supposedly cylindrical (Laplace law)

$$P_j r_j - P_{ic}(r_j + h_j) = T_{e,j} + T_{m,j} + T_{v,j} \quad j = 1, 2$$

where P_j is the intravascular pressure in the j th segment; P_{ic} is the extravascular (i.e., intracranial) pressure; h_j is wall thickness; and $T_{e,j}$, $T_{m,j}$, and $T_{v,j}$ denote elastic, smooth muscle, and viscous tensions, respectively.

Wall thickness is calculated as a function of inner radius, assuming that the vessel wall is incompressible; hence, its volume remains constant. Mathematical expressions for tensions have been given to reproduce results of experimental studies on isolated arterioles (10).

Examples of the tension-inner radius diagrams at steady-state conditions for proximal and distal pial arteries are shown in Fig. 2. The equilibrium points can be located on the curve for different working conditions. It can be seen that the percentage of radius change during maximal vasodilation is greater in the small pial arteries than in proximal arteries, in accordance with results of physiological experiments (6, 25, 29, 32, 53).

The geometric parameters characterizing the large and small pial arteries (i.e., inner radii in unstressed conditions and in basal conditions, thickness-to-radius ratio, and overall blood volume in basal conditions) have been set according to data reported previously (50, 51). The only difference is that, in the present model, the inner radius in the first segment is 10 times smaller than in previous studies. In fact, in earlier versions of the model, the first segment was representative not only of large pial vessels but also of basal cerebral arteries, both of which were assumed to be actively regulated by a pressure-dependent autoregulation mechanism (32). In this new model, however, with reference to more recent data (13, 36), we have assumed that the large basal arteries in the circle of Willis are not directly involved in the cerebral autoregulation response. Large basal arteries have therefore been treated as purely passive in nature.

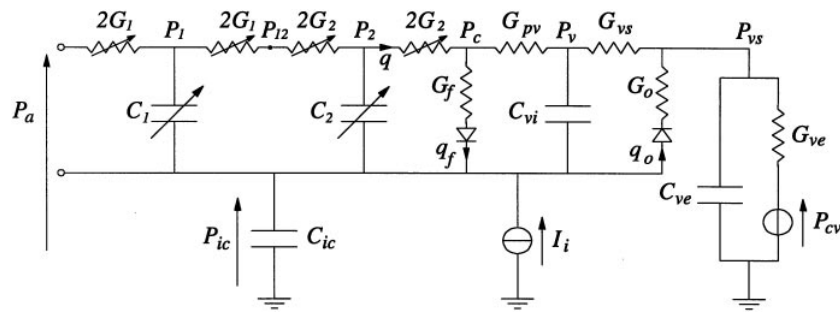


Fig. 1. Electric analog of intracranial dynamics. G_1 and C_1 , hydraulic conductance and compliance, respectively, of proximal cerebral arteries; G_2 and C_2 , hydraulic conductance and compliance, respectively, of distal cerebral arteries; P_a , systemic arterial pressure (SAP); P_1 and P_2 , intravascular pressure of large pial arteries and medium and small arteries, respectively; q , cerebral blood flow (CBF); P_c and P_v , capillary and cerebral venous pressure, respectively; P_{vs} and P_{cv} , sinus venous and central venous pressure, respectively; P_{ic} , intracranial pressure (ICP); C_{ic} , intracranial compliance; G_{pv} and C_{vi} , hydraulic conductance and compliance of large cerebral veins; G_{vs} , hydraulic conductance of terminal intracranial veins (bridge veins and lateral lacunae or lakes); G_{ve} and C_{ve} , hydraulic conductance and compliance, respectively, of extracranial venous pathways; G_f and G_o , conductances to cerebrospinal fluid (CSF) formation and CSF outflow; q_f and q_o , rates of CSF formation and CSF outflow; and I_i , artificial CSF injection rate.

The values of conductances in basal conditions have been assigned to reproduce a typical pressure distribution in the pial circulation as reported previously (50, 51).

Cerebral venous circulation. The circulatory pathway from cerebral capillaries down to the dural sinuses also consists of

a series arrangement of venous capacity and upstream and downstream longitudinal conductances. Because autoregulation plays a negligible role in cerebral veins (4), we adopted a simpler description for venous mechanics than for the pial arterial-arteriolar vasculature. The venous compliance (C_{vi}) is inversely dependent on the local transmural pressure, implying a monoexponential pressure-volume relationship. The terminal portion of the intracranial venous bed (bridge veins and lateral lacunae or lakes, represented by the conductance G_{vs} in the model) passively collapses or narrows during intracranial hypertension, with a mechanism similar to that of a Starling resistor (4, 33). Because of this mechanism, cerebral venous pressure (P_v) is always slightly higher than ICP, and upstream large cerebral veins and venules remain open during intracranial hypertension. Consequently, conductance of the proximal venous circulation (G_{pv}) is constant. The remaining part of the vascular bed, from dural sinuses down to the heart, is summarized by the hydraulic conductance (G_{ve}) and compliance (C_{ve}) of the extracranial venous pathways.

CSF compartment. We have assumed that the processes of both CSF production at the cerebral capillaries and CSF outflow at the dural sinuses are passive and unidirectional. Hence, they are proportional to the corresponding transmural pressure value and fall to zero when this becomes negative.

All the parameters that describe the venous and CSF compartments have been given the same basal values used in previous studies, for which thorough discussions of these quantities can be found (50, 51).

Middle cerebral artery blood flow velocity. Additional equations in the model have been included to estimate an approximate value for blood flow velocity in the middle cerebral artery (MCA) and to compare it with experimental data as recorded with the TCD technique. On the basis of studies conducted on healthy subjects and neurosurgical patients (13, 36), we assumed that the behavior of the MCA is essentially passive in nature; the transmural pressure (SAP - ICP) is a monoexponential function of the inner radius (Fig. 3). The parameters of this relationship have been set to reproduce the pressure-radius curves concerning human intracranial basal arteries (20). Finally, the MCA velocity (V_{MCA}) is calculated as the ratio of blood flow to vessel cross-sectional area. To this end, we assumed that about one-third of total CBF passes through each MCA. Based on these assumptions, the basal value of V_{MCA} in the model is as high as 60 cm/s, which agrees with the values reported by Aaslid et al. (1)

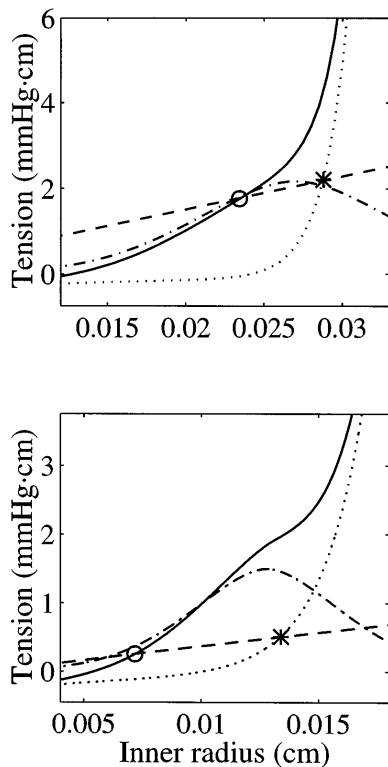


Fig. 2. Pattern of wall tension vs. inner radius in large (*top*) and small (*bottom*) pial arteries computed with model in steady-state basal conditions. As demonstrated by some authors (10), vessels of different sizes from a singular vascular bed have similar mechanical characteristics. Dotted line: elastic tension; dot-dashed line: active tension; continuous line: total tension. Dashed line represents tangential force per unit length, computed according to the Laplace law in basal conditions. ○ denotes basal value of inner radius at equilibrium; * denotes equilibrium level following vasodilation induced by complete smooth muscle relaxation, assuming constant intravascular and extravascular pressures. Note greater vasodilatory capacity of small pial arteries compared with large pial arteries.

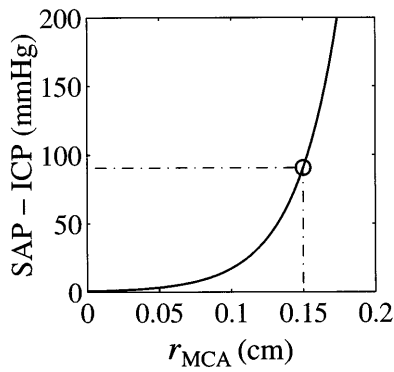


Fig. 3. Theoretical pattern of transmural pressure (SAP - ICP) vs. inner radius in middle cerebral artery (r_{MCA}). To qualitatively reproduce data reported in Ref. 20, we assumed a monoexponential pressure-radius relationship. \circ denotes basal working point at equilibrium, characterized by a transmural pressure of ~ 90 mmHg and an inner radius of 0.15 cm.

(normal range 33–90 cm/s, mean 62 cm/s). Furthermore, during maneuvers that affect SAP or CO₂ pressure, the V_{MCA} changes are in agreement with those measured with the TCD technique (see RESULTS). This aspect has been more deeply analyzed in a second, related paper (27).

Cerebrovascular Regulation Mechanisms

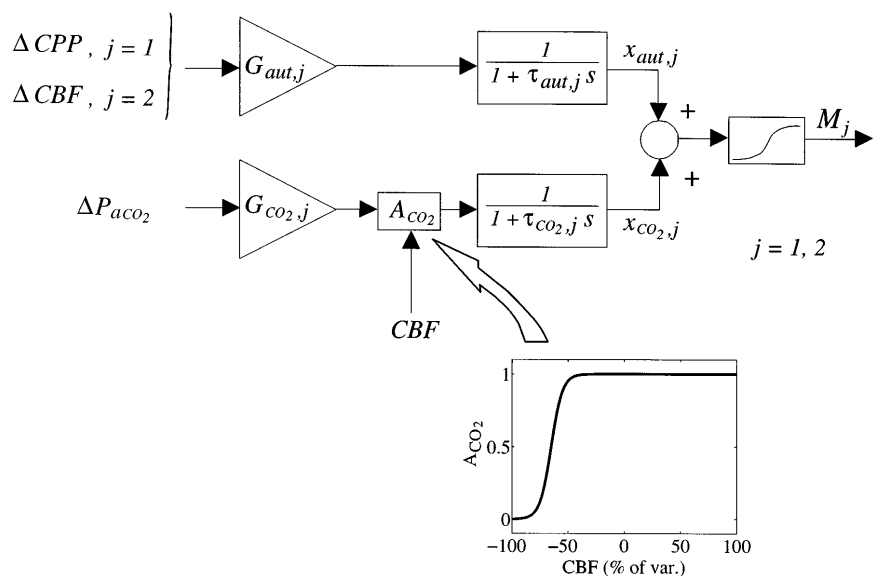
Cerebrovascular regulation mechanisms act on smooth muscle tension of large pial arteries and arterioles. To reproduce their action, we assumed that the amplitude of the “active tension-inner radius” relationship ($T_{max,j}$) depends on an activation factor (M_j) that represents the degree of smooth muscle contraction in the given segment. Hence

$$T_{max,j} = T_{max,0,j}(1 + M_j)$$

where $T_{max,0,j}$ is a constant parameter. The value $M_j = 0$ indicates basal conditions. When $M_j > 0$, there is active vasoconstriction, whereas $M_j < 0$ is associated with a condition of muscle relaxation and vasodilation.

The block diagram in Fig. 4 shows how feedback mechanisms modulate the activation factor. The upper branch refers to cerebrovascular autoregulation mechanisms, whereas the lower branch refers to CO₂ reactivity. The contributions of

Fig. 4. Block diagram shows how different regulatory mechanisms modify smooth muscle activation factor (M_j) of large ($j = 1$) and small ($j = 2$) pial arteries. *Upper branch* describes autoregulation mechanisms, whereas *lower branch* indicates CO₂ response. Input quantity for CO₂ mechanisms in both segments is logarithm of arterial CO₂ tension (Pa_{CO_2}), i.e., $\Delta Pa_{CO_2} = \log_{10}(Pa_{CO_2}/Pa_{CO_2,n})$, where $Pa_{CO_2,n}$ represents Pa_{CO_2} value that does not affect basal smooth muscle tension. In contrast, input quantity for autoregulation is different in the two segments: large pial arteries actively respond to changes in cerebral perfusion pressure (ΔCPP), whereas small pial arteries are sensitive to CBF percent changes (ΔCBF). Dynamics of each mechanism are simulated by means of a gain factor (G) and a first-order low-pass filter with time constant τ . Gain factor of CO₂ mechanisms is multiplied by corrective factor A_{CO_2} , which lowers CO₂ reactivity at low CBF levels (see *inset*) as a consequence of tissue ischemia. Finally, autoregulation and CO₂ mechanisms interact nonlinearly through a sigmoidal static relationship.



autoregulation and CO₂ reactivity to smooth muscle tension in the j th segment are described by two state variables, $x_{aut,j}$ and $x_{CO_2,j}$ respectively. The dynamics of each is reproduced by means of a first-order low-pass filter, characterized by a gain factor ($G_{aut,j}$ or $G_{CO_2,j}$) and a time constant ($\tau_{aut,j}$ or $\tau_{CO_2,j}$).

As shown in Fig. 4, we have assumed that autoregulation acts on large pial arteries and small arterioles by means of two distinct feedback mechanisms: the mechanism on large arteries depends on changes in CPP, reflecting a myogenic or neurogenic mechanism; and the mechanism on small arteries is triggered by alterations in blood flow to cerebral tissue, according to a metabolic or endothelium-dependent response. This distinction aims at reproducing the heterogeneity of autoregulation observed by Kontos et al. (25) and MacKenzie et al. (29) in cats.

In contrast, CO₂ is assumed to affect smooth muscle tension, in both large and small pial arteries, through a similar mechanism. Because the prevalent hypothesis ascribes the vasoactive effect of CO₂ to pH changes in the perivascular space (24, 34), we have assumed that model response depends on the logarithm of CO₂ changes rather than on Pa_{CO_2} by itself. Hence, the following input quantity is used in the block diagram in Fig. 4

$$\Delta Pa_{CO_2} = \log_{10} \frac{Pa_{CO_2}}{Pa_{CO_2,n}}$$

The parameter $Pa_{CO_2,n}$ denotes the level of CO₂ pressure that does not affect the basal smooth muscle tension. By changing this parameter, adaptation of cerebrovascular reactivity to prolonged hypercapnia or hypocapnia can be simulated (34, 39).

Furthermore, we have included two kinds of nonlinear interaction between autoregulation and CO₂ reactivity. First, on the basis of several experimental studies (8, 18), we have assumed that the strength of the CO₂ mechanism is not independent on CBF but, rather, is attenuated during severe brain ischemia. Ischemia, in fact, causes tissue acidosis, which has a buffer effect on the influence of CO₂ on perivascular pH. Accordingly, the CO₂ reactivity in the model decreases exponentially when CBF falls below normal (see *inset* in Fig. 4).

Second, Fig. 4 shows that autoregulation and CO₂ reactivity are not simply summed to obtain the activation factor (M_j);

rather, they interact through a sigmoidal relationship, which accounts for the existence of lower and upper limits for cerebrovascular reactivity.

A value characterizing the parameters in the sigmoidal relationship has been set so that smooth muscle tension falls to zero during maximal vasodilation and can rise to twice the basal value during maximum vasoconstriction.

The autoregulation time constants were set at the same values used in previous studies (50, 51). In particular, we assumed that the pressure-dependent mechanisms acting on large pial arteries exhibit rapid dynamics ($\tau_{\text{aut},1} = 10$ s), whereas the flow-dependent response of pial arterioles is slightly slower ($\tau_{\text{aut},2} = 20$ s).

The choice of time constants for CO₂ reactivity deserves further comment. Kontos et al. (24) found that arteriolar dilation in response to a pH decrease takes place rapidly, with a time constant of <10 s. Schneider et al. (43), during experiments on feline pial arteries with the use of a microelectrode, observed that pH and vascular diameter varied with a delay of ~30 and 45 s, respectively, after a CO₂ change; Severinghaus and Lassen (45) reported a time constant of 20 s for CO₂ reactivity in humans, whereas Auer (3) in his study on cats measured a delay between 7 and 48 s. It is worth noting that, in the last three cases, the measured quantity was the end-tidal CO₂ pressure; the observed delays therefore also included the transit time for blood to pass from the lung to the brain. Because in our model the input quantity is the arterial CO₂ pressure, the time constant includes only the time necessary for Pa_{CO₂} to alter perivascular pH and that required for the vessel to react to a pH change. Hence, we have chosen a value of $\tau_{\text{CO}_2,j} = 20$ s for both large and small pial arteries. In the analysis of neurosurgical patients reported in our related paper (27), we have used a greater value for the parameter $\tau_{\text{CO}_2,j}$ because the monitored quantity is end-tidal rather than arterial CO₂ pressure.

Values for the gain factors of regulation mechanisms have been set to reproduce results obtained in animals when experiments are executed at constant ICP (see RESULTS).

A list of all model parameters and their values at basal conditions can be found in Table 1.

RESULTS

Model simulations have been performed to analyze 1) cerebral autoregulation, 2) CO₂ reactivity, 3) the interactions between these two mechanisms, and 4) the effect of acute changes in CO₂ on ICP. With regard to the first three topics, only results obtained under steady-state conditions are presented and compared with experimental data. Moreover, to simulate experiments performed with the dura opened or at constant ICP, during these trials we used an extremely low value for the intracranial elastance coefficient. Hence, ICP changes were negligible throughout the simulations (ICP ≈ 9.5 mmHg). In contrast, the last trials concern dynamic conditions, with ICP free to change as a consequence of blood volume and CSF volume alterations.

Cerebral Autoregulation

Figure 5 shows the percent changes in inner radii in large and small pial arteries, percent change in CBF, and percent change in V_{MCA} evaluated under steady-state conditions at different values of mean SAP. A value was applied to the parameters that describes the

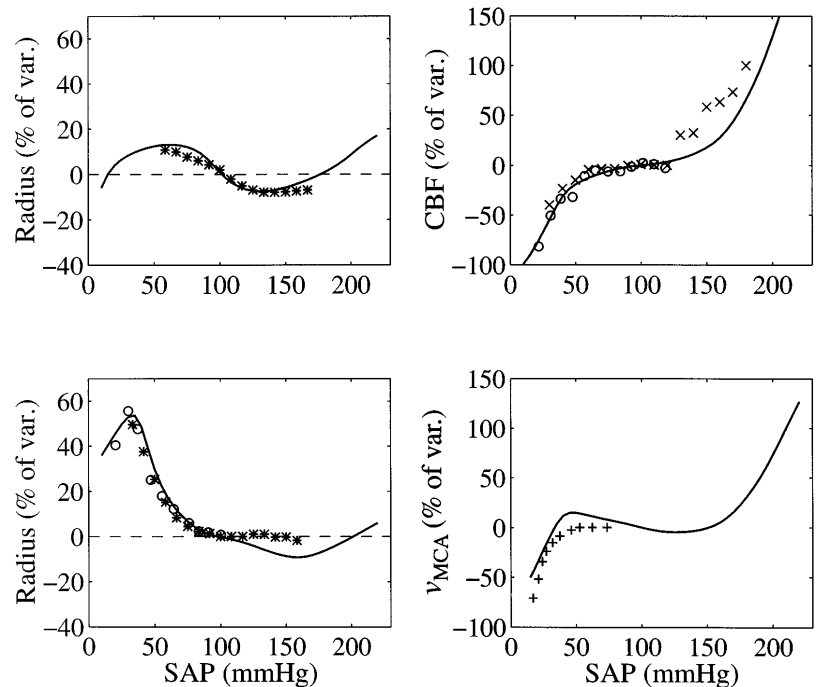
Table 1. Values of model parameters in basal conditions

Parameter Values		
$r_{\text{MCA}n} = 0.15$ cm		
$K_{\text{MCA}} = 5$		
$r_{0,1} = 0.015$ cm		$r_{0,2} = 0.0075$ cm
$h_{0,1} = 0.003$ cm		$h_{0,2} = 0.0025$ cm
$\sigma_{e0,1} = 0.1425$ mmHg		$\sigma_{e0,2} = 11.19$ mmHg
$K_{r,1} = 10$		$K_{r,2} = 4.5$
$\sigma_{\text{coll},1} = 62.79$ mmHg		$\sigma_{\text{coll},2} = 41.32$ mmHg
$T_{\text{max},1} = 2.16$ mmHg·cm		$T_{\text{max},2} = 1.50$ mmHg·cm
$r_{m,1} = 0.027$ cm		$r_{m,2} = 0.0128$ cm
$r_{t,1} = 0.018$ cm		$r_{t,2} = 0.0174$ cm
$n_{m,1} = 1.83$		$n_{m,2} = 1.75$
$\eta_1 = 2.32 \times 10^2$ mmHg·s		$\eta_2 = 0.478 \times 10^2$ mmHg·s
$K_{G,1} = 1.43 \times 10^6$ (mmHg·s·cm) ⁻¹		$K_{G,2} = 1.02 \times 10^8$ (mmHg·s·cm) ⁻¹
$K_{V,1} = 4.64 \times 10^3$ cm		$K_{V,2} = 154.32 \times 10^3$ cm
	$G_{\text{pv}} = 1.136$ mmHg ⁻¹ ·s ⁻¹ ·ml	
	$k_{\text{ven}} = 0.31$ ml ⁻¹	
	$P_{v1} = -2.5$ mmHg	
	$G'_{\text{vs}} = 2.77$ mmHg ⁻¹ ·s ⁻¹ ·ml	
	$G_{\text{ve}} = 6.251$ mmHg ⁻¹ ·s ⁻¹ ·ml	
	$C_{\text{ve}} = 2.34$ mmHg ⁻¹ ·ml	
	$P_{\text{cv}} = 4$ mmHg	
	$G'_{\text{r}} = 4.2 \times 10^{-4}$ mmHg ⁻¹ ·s ⁻¹ ·ml	
	$G_0 = 1.9 \times 10^{-3}$ mmHg ⁻¹ ·s ⁻¹ ·ml	
	$k_E = 0.11$ ml ⁻¹	
$\tau_{\text{aut},1} = 10$ s		$\tau_{\text{aut},2} = 20$ s
$G_{\text{aut},1} = 0.020$ mmHg ⁻¹		$G_{\text{aut},2} = 5.2$
$\tau_{\text{CO}_2,1} = 20$ s		$\tau_{\text{CO}_2,2} = 20$ s
$G_{\text{CO}_2,1} = 1.3$		$G_{\text{CO}_2,2} = 15.5$
	$K_{\text{CO}_2} = 20$	
	$b_{\text{CO}_2} = 0.65$	
$M_{\text{min},1} = -1$		$M_{\text{min},2} = -1$
$M_{\text{max},1} = 1$		$M_{\text{max},2} = 1$
	$P_{\text{an}} = 100$ mmHg	
	$P_{\text{vn}} = 14$ mmHg	
	$q_n = 12.5$ ml·s ⁻¹	
	$P_{\text{icn}} = 9.5$ mmHg	
	$\text{Pa}_{\text{CO}_2n} = 40$ mmHg	

Subscripts 1 and 2 in paired parameters refer to large pial arteries (proximal segment) and small pial arteries (distal segment) of cerebrovascular bed. Refer to text for parameter definitions.

autoregulation gain in both segments (i.e., $G_{\text{aut},j}$ in Fig. 4 and Eqs. 23A and 24A in APPENDIX) to reproduce the inner radius percent changes measured by Kontos et al. (25) and MacKenzie et al. (29) on animals; the correspondence is quite good. The results show that the importance of each pial segment depends on the arterial pressure level. During moderate SAP alterations, the changes in vessel caliber are more pronounced in the large pial arteries than in the arterioles. When arterial pressure is further decreased and approaches the autoregulation lower limit, dilation of small pial arteries becomes progressively greater, causing an enlargement of the cerebrovascular volume, whereas the response of

Fig. 5. Percent changes in inner radius of large (*top left*) and small (*bottom left*) pial arteries and percent changes in CBF (*top right*) and MCA velocity (V_{MCA} ; *bottom right*) evaluated with model in steady-state conditions at different mean SAP levels. Throughout simulations, ICP was set at a constant level (~ 9.5 mmHg). Model results (continuous lines) are compared with experimental data reported by Kontos et al. (25) in cats (*), MacKenzie et al. (29) in cats (O), Harper et al. (19) in rats (x), and Nelson et al. (35) in rabbits (+).



the larger vessels is rapidly exhausted. At very low or very high values of mean SAP, the inner radii behave in a completely passive way. The simulated pattern of CBF and V_{MCA} versus mean SAP also agrees with that of experimental data (19, 29, 35). Autoregulation is able to maintain a fairly constant CBF in the range of 50–150 mmHg (38); V_{MCA} does not decrease because of the passive variation in cross-sectional area (see Eq. 21A in APPENDIX). This result agrees with Nelson et al. (35), who found that velocity is always higher than CBF. Beyond the lower limit of autoregulation, CBF and V_{MCA} start to decrease, despite the evident vasodilation of the small pial arteries.

CO₂ Reactivity

Figure 6 shows the dependence of inner radii, CBF, and V_{MCA} on P_{aCO_2} under steady-state conditions. The value indicating normocapnia has been fixed at $P_{aCO_2} = 40$ mmHg. Also in this case, a value for the gain factors describing CO₂ reactivity (i.e., $G_{CO_2,j}$ in Fig. 4 and Eq. 25A in APPENDIX) was set to reproduce the inner radius percent changes observed during experiments on animals. The comparison between simulation results and the corresponding experimental and clinical data proves to be suitable (18, 26, 30, 40, 41, 44, 53). Also in this condition, as during autoregulation, the amount of vessel variation is more pronounced in the small pial arteries than in the large pial arteries. This finding agrees with the observation made by Wei et al. (53), who demonstrated that the CO₂ reactivity in the arterioles of cats is dependent on vessel size. Moreover, the vasoconstrictive effect of hypocapnia reduces CBF to one-half its normal value. During hypercapnia, vasodilation can even double CBF. V_{MCA} percent changes closely resemble those in CBF.

Interaction Between Autoregulation and CO₂ Reactivity

Figure 7 (*bottom*) shows the percent changes in small pial artery radius induced by arterial hypotension during normocapnia and hypercapnia. Figure 7 (*top*) displays the difference between vessel diameters during normocapnia and hypercapnia, which is considered an index of the CO₂ reactivity at different arterial pressure levels. As the model (Fig. 7, *left*) clearly shows, CO₂ reactivity initially increases with lowering mean SAP; afterward, when vasodilation in the small pial vessels becomes appreciable, CO₂ reactivity rapidly decreases. These findings qualitatively concur with the data reported by Wei et al. (53) (Fig. 7, *right*). The behavior shown in Fig. 7 can be attributed to the presence of nonlinear sigmoidal interaction between the two mechanisms that reflects the existence of upper and lower saturation levels for smooth muscle tension (see block diagram in Fig. 4).

Figure 8 describes the dependence of CBF on mean SAP (autoregulation curve) under steady-state conditions at various P_{aCO_2} levels. Obviously, an increase in P_{aCO_2} causes an increase in CBF at a given arterial pressure value. At the same time, the lower autoregulation limit shifts toward higher pressure; in fact, cerebral vessels are nearly maximally dilated because of hypercapnia and therefore are unable to dilate further in response to arterial hypotension. These findings are confirmed by several authors who studied the effects of induced hypotension at various P_{aCO_2} levels (16, 17, 37, 39).

Figure 9 describes the effect of arterial hypotension on the relationship between CBF and P_{aCO_2} . Model results are compared with those obtained by Harper

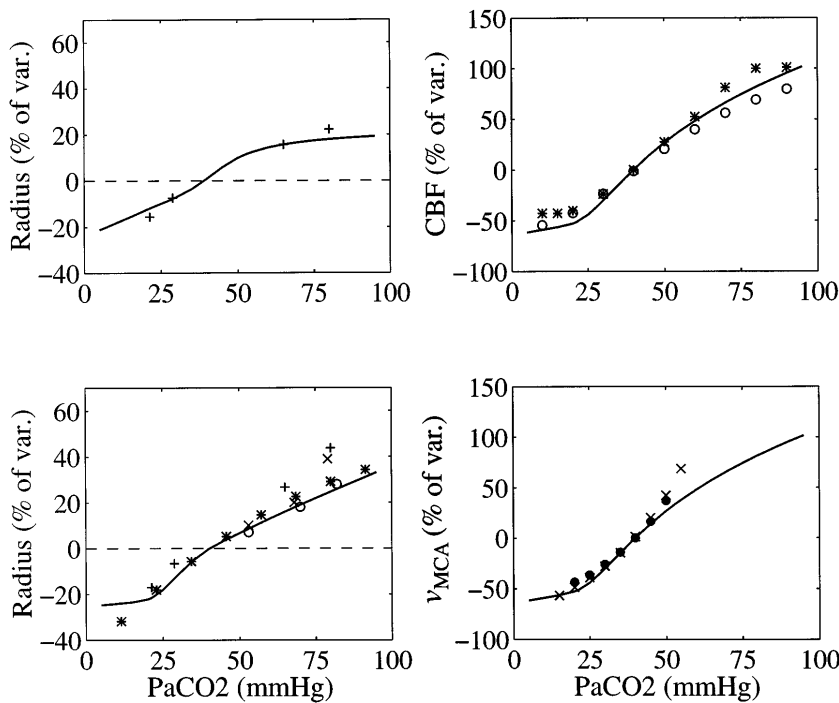


Fig. 6. Percent changes in inner radius of large (*top left*) and small (*bottom left*) pial arteries and percent changes in CBF (*top right*) and V_{MCA} (*bottom right*) evaluated with model in steady-state conditions at different levels of Pa_{CO_2} . Throughout simulations, ICP was set at a constant level (~ 9.5 mmHg). Model results (continuous lines) are compared with experimental data reported by Wei et al. (53) in cats (+), Raper et al. (40) in cats (*), and Levasseur and Kontos (26) in rabbits (O, X) for radii; with data from Reivich (41) in monkeys (O) and Harper and Glass (18) in dogs (*) for CBF; and with data from Markwalder et al. (30) in healthy human subjects (X) and Seiler and Nirkko (44) in clinical patients (●) for V_{MCA} .

and Glass (18) during experiments on dogs. It can be seen that arterial hypotension progressively reduces CO₂ reactivity. The most considerable effect of hypotension is visible during hypercapnia, when the arterial bed is already dilated to the maximum. On the other hand, experimental data suggest that the vasoconstrictory effect of hypocapnia is also reduced during severe hypotension (18). The model can reproduce this behavior, attributing it to a reduction in the CO₂ reactivity

during cerebral ischemia (see block diagram in Fig. 4 and *Eqs. 25A* and *26A* in APPENDIX).

Effects of Hypocapnia and Hypercapnia on ICP

The purpose of the following simulations, performed with ICP free to change, is to analyze the possible effects of CO₂ variations on ICP in patients with head injuries. This matter has been analyzed in depth in a second, related paper (27). We shall consider a hypothetical patient with moderate increase in CSF outflow resistance, hence with moderate intracranial hypertension. Three different cases, characterized by a progressive reduction in craniospinal elasticity, are presented.

Figure 10 shows the ICP response to an acute rise in Pa_{CO_2} . Hypercapnia causes a vasodilation with an increase in CBV, leading to a sudden ICP rise; subse-

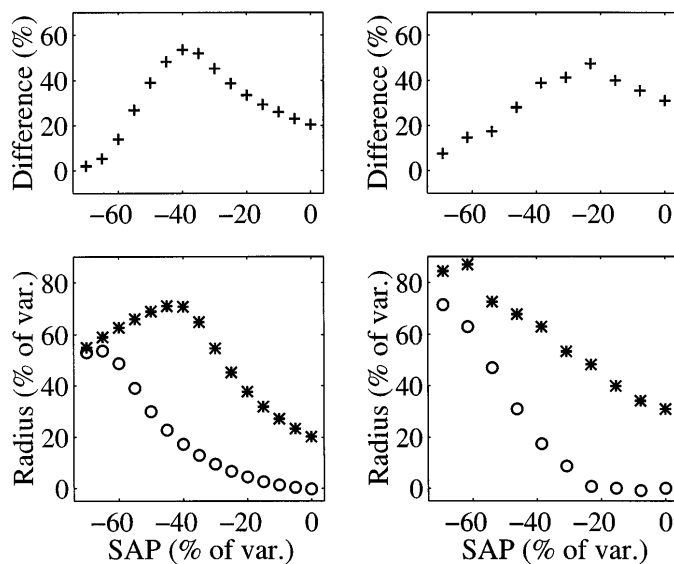


Fig. 7. *Bottom*: percent changes in inner radius in small pial arteries (distal segment) vs. mean SAP during normocapnia (O, $Pa_{CO_2} = 40$ mmHg) and hypercapnia (*, $Pa_{CO_2} = 71$ mmHg). *Top*: percent difference between vessel radius during hypercapnia and normocapnia at same arterial pressures. Model results (*left*) are compared with experimental data by Wei et al. (53) in cats (*right*). Throughout simulations, ICP was set at a constant level (~ 9.5 mmHg).

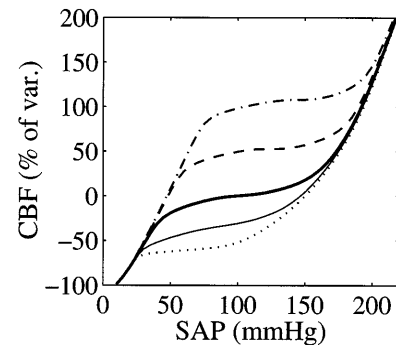


Fig. 8. Effect of hypocapnia and hypercapnia on CBF. Pattern of CBF vs. mean SAP (autoregulation) was simulated with model in steady-state conditions at different levels of Pa_{CO_2} (dotted line: 20 mmHg; continuous fine line: 30 mmHg; continuous bold line: 40 mmHg; dashed line: 60 mmHg; dot-dashed line: 90 mmHg). Note that hypercapnia shifts lower autoregulation limit toward higher pressures.

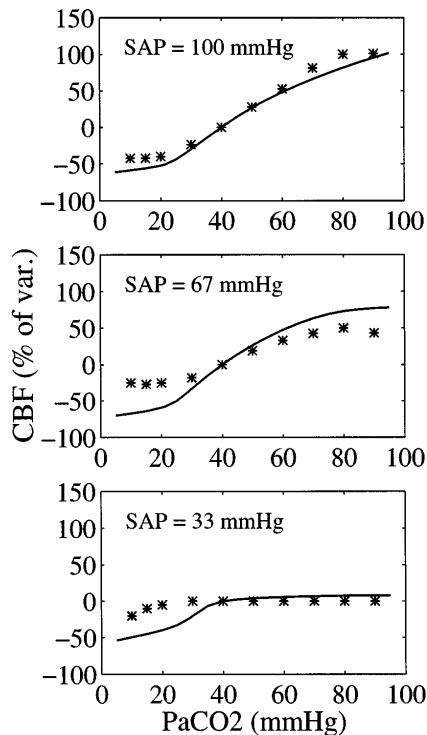


Fig. 9. Effect of hypotension on CBF. Percent changes in CBF vs. PaCO₂ were simulated with model in steady-state conditions at different mean SAP levels. All simulations were performed at constant ICP (~9.5 mmHg). Model results (continuous lines) are compared with experimental data (*) collected by Harper and Glass (18) in dogs.

quently, however, ICP returns monotonically toward baseline due to CSF reabsorption. The final ICP value remains slightly high with respect to the initial situation because, in the model, the increase in CBF causes a parallel increase in CSF production rate. As intracranial compliance diminishes, the capacity to buffer CBV variations decreases, and ICP shows a dramatic transient rise. In the extreme case, the ICP pattern resembles that of the single A wave or plateau wave observed by Lundberg (28).

In Fig. 11 the ICP reaction to induced hypocapnia is plotted. The conditions are similar to those in Fig. 10; in this case, however, CO₂ change produces a clear drop in ICP that is partially recovered by the process of CSF production. The final ICP level is lower than the initial level due to a decrease in CSF production rate. Also in this case, the lower the craniospinal storage capacity, the greater the ICP alteration.

DISCUSSION

The present work improves our previous model significantly, including the analysis of CO₂ cerebrovascular reactivity and the interaction among CO₂, autoregulation, and ICP. The model aims at representing an acceptable compromise between physiological accuracy and clinical usefulness. In fact, even though the emphasis of this study is on the modeling of physiological experiments, an understanding of the pathophysiology

of intracranial dynamics is an essential prerequisite in the treatment of severe brain diseases.

An important methodological aspect of this study is that many different experimental results, concerning various phenomena of intracranial dynamics often considered separately in the literature, can be summarized into a single theoretical setting. The main aspects elucidated in this work are discussed separately below.

Cerebrovascular Segmental Heterogeneity

A critical choice in the model concerns the subdivision of the cerebrovascular bed into several consecutive segments, each characterized by its own parameters and a specific functional response to pressure and/or CO₂ changes. Our segmentation largely concurs with that proposed by Kontos and colleagues (25, 53); these authors observed a vessel-size dependence in the response to blood pressure and CO₂ changes between small and large pial arteries. This different behavior of the pial vascular bed, confirmed in other studies (29, 32), is shown by our model to be a mere consequence of the Laplace law and of the different values of intravascular pressure at consecutive levels of the pial vasculature.

Moreover, in this study, as in a previous one (51), we assumed that autoregulation of the large pial artery is dominated by pressure-dependent mechanisms, whereas the response of small pial arteries mainly depends on blood flow changes. This hypothesis permitted us to reproduce not only the active response of the vessels quite well but also all CBF and V_{MCA} changes at many levels of arterial pressure and CO₂. Hence, we are confident that this subdivision into two regulated seg-

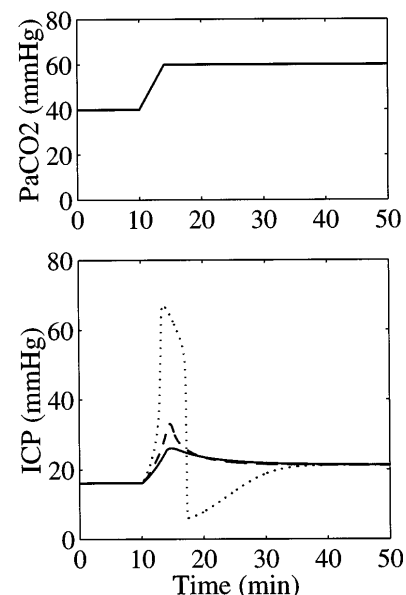


Fig. 10. Effect of hypercapnia on ICP. Time pattern of ICP (bottom) was simulated with model in response to a sharp PaCO₂ increase from 40 to 60 mmHg (top) in a patient with a moderate decrease in CSF outflow conductance ($G_0 = 6.33 \times 10^{-4} \text{ mmHg}^{-1} \cdot \text{s}^{-1} \cdot \text{ml}$); i.e., with moderate intracranial hypertension during normocapnia. Results of 3 different simulations are shown, assuming normal intracranial compliance (continuous line; $k_E = 0.11 \text{ ml}^{-1}$), moderately reduced intracranial compliance (dashed line; $k_E = 0.143 \text{ ml}^{-1}$), and severely reduced intracranial compliance (dotted line; $k_E = 0.22 \text{ ml}^{-1}$).

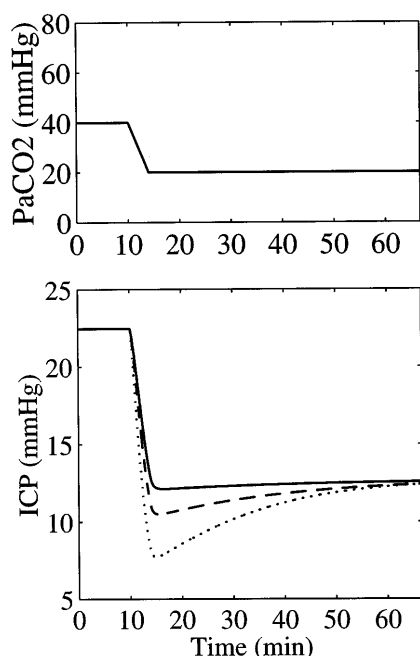


Fig. 11. Effect of hypocapnia on ICP. Time pattern of ICP (*bottom*) was simulated with model in response to a sharp Pa_{CO₂} decrease from 40 to 20 mmHg (*top*) in a patient with a moderate decrease in CSF outflow conductance ($G_0 = 3.80 \times 10^{-4} \text{ mmHg}^{-1} \cdot \text{s}^{-1} \cdot \text{ml}$); i.e., with moderate intracranial hypertension during normocapnia. Results of 3 different simulations are shown, assuming normal intracranial compliance (continuous line; $k_E = 0.11 \text{ ml}^{-1}$), moderately reduced intracranial compliance (dashed line; $k_E = 0.143 \text{ ml}^{-1}$), and severely reduced intracranial compliance (dotted line; $k_E = 0.22 \text{ ml}^{-1}$).

ments actually represents the best compromise between accuracy and simplicity and allows cerebrovascular reactivity to be reproduced with a limited number of parameters. Moreover, the good correlation between model and experimental CBF data confirms the minor role that the venous cerebrovascular bed plays in CBF regulation.

Cerebrovascular Response to CO₂

The genesis of CO₂ reactivity has been discussed in many papers over recent decades (24, 34, 43, 45, 46). Some authors hypothesized that the effect of CO₂ on cerebral vessels is mediated by a neurogenic mechanism, probably involving the brain stem (9, 12, 46). However, most experimental results suggest that CO₂ reactivity is mediated principally by local factors, mainly pH changes in the perivascular space (24, 34, 43). Accordingly, we assumed a logarithmic relationship between smooth muscle tension and CO₂ pressure to emphasize that vessel response depends on perivascular pH rather than on CO₂ pressure per se. This relationship allowed us to reproduce various experimental and clinical results concerning vessel caliber percent changes, CBF, and V_{MCA} variations during hypercapnia and hypocapnia (18, 26, 30, 35, 40, 41, 44, 53).

It is well known that CO₂ reactivity tests are frequently conducted on neurosurgical patients to assess cerebral vessel vasomotor capacity (8, 12, 48). Usually CO₂ reactivity is quantified by an index equal to CBF percent changes per mmHg of Pa_{CO₂} change. We as-

sessed the sensitivity of CBF to CO₂ variations in the model by computing the central slope of the curve shown in Fig. 6. The value obtained is $\sim 2.5\%$ CBF change/mmHg Pa_{CO₂} change. This value quite closely concurs with those obtained during physiological experiments on animals [2.2%/mmHg by Jones et al. (23) in rats; 2.1%/mmHg by Göbel et al. (15) in rats; and 2.87%/mmHg by D'Alecy et al. (9) in dogs]. With regard to human subjects, Tenjin et al. (48) suggested the value 2.0%/mmHg as a threshold to discriminate between patients with preserved and impaired CO₂ reactivity.

Interaction Between Autoregulation and CO₂ Response

An important aspect of CBF control, documented in many physiological and clinical studies, is the presence of a significant nonlinear interaction between CO₂ reactivity and autoregulation. Simulating the nature of this interaction is not only a problem of physiological importance but also is one that may have a great clinical impact. First, it is generally accepted that CO₂ reactivity is an important prognostic index significantly correlated with clinical outcome. Nevertheless, knowledge of this index alone may be misleading if not integrated with information on arterial pressure, CBF, and autoregulation status. Second, hyperventilation is an effective means routinely used to control ICP in neurosurgical patients. However, the effectiveness of this maneuver hinges on mean SAP and autoregulation, a fact that should be kept in mind by clinicians when planning patient treatment (12). Finally, anyone trying to identify the parameters characterizing CBF control (e.g., the gains and time constants of the mechanisms) needs to consider their complex interactions and nonlinear "inhibitory-facilitatory" summation. The latter problem is addressed in the second, related paper (27).

Several experimental results show that arterial hypotension can critically interfere with the cerebrovascular response to CO₂ changes. Harper and Glass (18), in a classic study, demonstrated that reducing arterial pressure to about one-third that of normal completely eliminates the vasodilatory response to hypercapnia and seriously weakens the vasoconstrictory response to hypocapnia. The latter result was further confirmed by others (2, 3).

A thorough analysis of the interaction between autoregulation and hypercapnia on pial vessel response can be found in the study by Wei et al. (53). According to their findings (see Fig. 7), the interaction between the two mechanisms is significantly nonlinear, i.e., the superimposition of the effects does not hold. In particular, as blood pressure decreases starting from a basal level, the responsiveness to CO₂ becomes initially greater, suggesting a "facilitatory" overlapping of the two mechanisms. However, when arterial pressure approaches the autoregulation lower limit, CO₂ responsiveness progressively disappears, indicating an "inhibitory" overlapping of autoregulation and hypercapnia.

It is well known that hypercapnia and hypocapnia significantly modulate the autoregulation curve. Hyper-

capnia shifts the autoregulation plateau to higher CBF levels, and hypocapnia reduces it to a lower CBF. Moreover, data collected by several authors concur, showing that the lower autoregulation limit is fairly shifted by CO₂ changes (16, 17, 37, 39). More controversial results can be found for the effect of CO₂ on the upper limit of autoregulation (11, 16, 38).

We were able to qualitatively reproduce most of the results mentioned above (Figs. 7–9) by supposing the presence of only two significant nonlinearities in the interaction between autoregulation and CO₂ response. Both nonlinearities are confirmed by physiological considerations.

A first nonlinearity in the model derives from a sigmoidal static relationship and accounts for the natural bounds of smooth muscle tension (see last block in Fig. 4) and permits reproduction of most of the nonlinearities observed during combined stimuli. However, the presence of this sigmoidal relationship for smooth muscle tension did not allow us to explain the lack of vasoconstrictory response to hypocapnia observed during severe arterial hypotension (2, 3, 18). It has been claimed that the failure of cerebral vessels to constrict to hypocapnia during hypotension indicates that maintenance of adequate tissue O₂ supply prevails over the maintenance of adequate CO₂ and acid-base levels (18). To account for this phenomenon, we assumed that cerebrovascular CO₂ reactivity depends on CBF through a sharply nonlinear relationship (see *inset* in Fig. 4); when CBF falls below an alarm threshold (indicating the initiation of ischemia), CO₂ reactivity is suddenly withdrawn. As a consequence of this assumption, cerebrovascular response to hypocapnia progressively disappears when mean SAP decreases below the autoregulation lower limit (SAP < 50 mmHg) in accordance with data by Artru and Colley (2). The existence of an “ischemic threshold” for CBF, below which CO₂ reactivity drops to zero, is also confirmed by clinical observations (8).

Interaction Between CBF Control and ICP

The existence of a close relationship among the action of CBF control mechanisms, cerebral blood volume changes, ICP, and intracranial dynamics is a peculiar characteristic of cerebrovascular regulation that is not shared by other vascular beds. This has been stressed by several authors in past years, beginning with the pioneering works by Lundberg (28), up to the fundamental studies that appeared in the mid-1980s by Rosner and Becker (see e.g., Ref. 42). Using a previous version of the present model (51), we were able to support most of Rosner’s ideas; the model predicted in pathological conditions the generation of self-sustained ICP oscillations very similar to plateau waves. This is a result of a potential positive feedback among autoregulation, CBV changes, and ICP, called by those authors “vasodilatory cascade.”

The new simulation results presented in Figs. 10 and 11 confirm the existence of a similar vasodilatory cascade in response to maneuvers that alter CO₂ concen-

tration in blood. Two main aspects of these simulations deserve consideration. First, the impact of CO₂ changes on ICP crucially depends on the status of intracranial compensatory mechanisms (CSF outflow and intracranial elastance). The same maneuver, with almost no effect on ICP in physiological conditions, can potentially induce dramatic ICP changes in pathological states characterized by reduced CSF outflow and poor intracranial capacity. In the worst conditions, even a mild hypercapnia can induce a disproportionate transient ICP rise, similar to that of a single plateau wave, with the risk of acute intracranial hypertension and cerebral ischemia (Fig. 10).

Furthermore, the results of Fig. 11 indicate how hyperventilation can be used to control ICP in patients at risk of intracranial hypertension. It should be noted that, in our model, the effect of CO₂ changes on ICP depends on two concurrent mechanisms that usually operate with different time constants: 1) active CBV changes, which cause rapid alterations in ICP, generally within a minute of the maneuver; and 2) alteration in CSF production rate, which takes place with a longer time constant (several minutes) and contributes to set the final steady-state ICP level. In the model, CSF production rate depends on capillary pressure and is therefore proportional to CBF.

An important new aspect of this model concerns the relationship between CBF and V_{MCA} . In this study we assumed that the MCA behaves passively, i.e., its inner radius is a monotonic function of transmural pressure; neither autoregulation nor CO₂ significantly affects the caliber of the MCA in the model. The consequence of such an assumption is that, during moderate variations in arterial pressure, velocity does not decrease, unlike CBF, due to variations in cross-sectional area. This behavior is supported by the experimental results by Nelson et al. (35) in the rabbit. In contrast, during CO₂ alterations, the velocity percent changes are of the same order as CBF changes, because transmural pressure and cross-sectional area in the large arteries remain almost unaffected. This model behavior agrees with data reported previously (30, 44). It is possible, however, that a different behavior for the MCA (inner radius being dependent on Pa_{CO₂}, or on an active myogenic response) may have significant consequences on model performance.

In perspective, the possibility of simulating the time pattern of ICP and TCD velocity in response to maneuvers affecting CO₂ and/or mean SAP could be used to estimate the main parameters of intracranial dynamics from measurements taken in neurosurgical intensive care units. On the basis of knowledge of these parameters in the individual patient, a greater understanding of pathophysiological mechanisms can be achieved and a more well-founded treatment for severe brain damage developed. This model application on real velocity and ICP tracings is the subject of a second, related study (27).

APPENDIX

Quantitative Model Description

Cerebral hemodynamics and CSF dynamics. The fundamental equations describing cerebral hemodynamics are written by imposing volume preservation equations at all nodes of Fig. 1.

Volume balance at the proximal arterial segment (large pial arteries) is

$$G_1(P_a - P_1) - \frac{G_1 G_2}{G_1 + G_2}(P_1 - P_2) = \frac{1}{2} \left(\frac{dV_1}{dt} \right) \quad (1A)$$

where G_1 and G_2 are the hydraulic conductances of proximal and distal arterial segments, respectively; P_a is mean cerebral arterial pressure (assumed equal to SAP); P_1 and P_2 are the intravascular pressures in the representative sections of large and small pial arteries; and V_1 is blood volume contained in the proximal segment.

Volume balance at the distal arterial segment (small pial arteries) is

$$\frac{G_1 G_2}{G_1 + G_2}(P_1 - P_2) - G_2(P_2 - P_c) = \frac{1}{2} \left(\frac{dV_2}{dt} \right) \quad (2A)$$

where P_2 is intravascular pressure at the representative section of pial arterioles, V_2 is blood volume contained in the distal arterial segment, and P_c is cerebral capillary pressure.

Volume balance at the cerebral capillaries is

$$2G_2(P_2 - P_c) - G_{pv}(P_c - P_v) = G_f(P_c - P_{ic}) \cdot H(P_c - P_{ic}) \quad (3A)$$

where G_{pv} is the hydraulic conductance in the proximal segment of cerebral veins, P_v is cerebral venous pressure, P_{ic} is intracranial pressure, and G_f is the conductance to CSF production. It should be noted that the right-hand member of Eq. 3A represents the CSF production rate from cerebral capillaries; we used the Heaviside function [$H()$], represented by means of a diode in the electric analog, to indicate that CSF production rate is unidirectional.

Volume balance at the large cerebral veins is

$$G_{pv}(P_c - P_v) - G_{vs}(P_v - P_{vs}) = C_{vi} \left(\frac{dP_v}{dt} - \frac{dP_{ic}}{dt} \right) \quad (4A)$$

where G_{vs} is the hydraulic conductance of the terminal venous vascular bed, including the lateral lakes and the bridge veins, P_{vs} is sinus venous pressure, and C_{vi} is intracranial venous compliance. The right-hand member of Eq. 4A represents blood volume changes in the venous vascular bed.

Volume balance at the dural sinuses is

$$G_{vs}(P_v - P_{vs}) + G_0(P_{ic} - P_{vs}) \cdot H(P_{ic} - P_{vs}) = G_{ve}(P_{vs} - P_{cv}) + C_{ve} \left(\frac{dP_{vs}}{dt} \right) \quad (5A)$$

where G_0 is the conductance to CSF outflow and G_{ve} and C_{ve} are the conductance and compliance, respectively, of the extracranial venous drainage pathways down to the central venous pressure (P_{cv}). The second term in the left-hand member of Eq. 5A represents the CSF reabsorption rate at the dural sinuses, which is assumed to be passive and unidirectional. The right-hand member of Eq. 5A denotes blood flow in the extracranial veins.

CONSTANCY OF OVERALL CRANIOSPINAL VOLUME (MONRO-KELLIE DOCTRINE). Imposing the balance of the total craniospinal volume, we obtain

$$C_{ic} \left(\frac{dP_{ic}}{dt} \right) = \frac{1}{k_E \cdot P_{ic}} \left(\frac{dP_{ic}}{dt} \right) = \frac{dV_1}{dt} + \frac{dV_2}{dt} + G_f(P_c - P_{ic}) \cdot H(P_c - P_{ic}) + C_{vi} \left(\frac{dP_v}{dt} - \frac{dP_{ic}}{dt} \right) - G_0(P_{ic} - P_{vs}) \cdot H(P_{ic} - P_{vs}) + I_i \quad (6A)$$

where, according to the previous equations, the first five terms in the right-hand member of Eq. 6A represent blood volume changes in the proximal and distal arterial segments, CSF production rate, volume changes in the cerebral veins, and CSF reabsorption rate, respectively. Finally, I_i denotes the amount of artificial CSF injected into (if positive) or subtracted from (if negative) the craniospinal space during clinical maneuvers (PVI tests).

Finally, a value characterizing CBF (q) can be computed as the product of conductance and pressure drop in any longitudinal segment (CSF circulation being negligible compared with CBF). By considering the segment of small pial arteries, we have

$$q = 2G_2(P_2 - P_c) \quad (7A)$$

Biomechanics of arterial-arteriolar cerebrovascular bed. In Eq. 8A, subscript $j = 1$ denotes a quantity belonging to the segment of large pial arteries, whereas subscript $j = 2$ refers to pial arterioles.

The equilibrium of tangential forces in a vessel wall is provided by the Laplace law

$$P_j r_j - P_{ic}(r_j + h_j) = T_{e,j} + T_{m,j} + T_{v,j} \quad j = 1, 2 \quad (8A)$$

where r is inner radius, h is wall thickness, and T_e , T_m , and T_v represent elastic, smooth muscle (active), and viscous tensions (force per unit length), respectively.

Elastic stress (force per unit surface) increases exponentially with inner radius, reflecting the behavior of elastin and collagen fibers in the wall. Hence we have

$$\sigma_{e,j} = \sigma_{e,0,j} \left[\exp \left(K_{\sigma,j} \cdot \frac{r_j - r_{0,j}}{r_{0,j}} \right) - 1 \right] - \sigma_{coll,j} \quad j = 1, 2 \quad (9A)$$

$$T_{e,j} = \sigma_{e,j} h_j \quad j = 1, 2 \quad (10A)$$

where σ_e is elastic stress, r_0 is the inner radius in the condition of "unstressed wall," and K_σ , σ_0 , and σ_{coll} are constant parameters. In particular, σ_{coll} has been introduced to permit the vessel to sustain a moderate negative tension before collapsing.

Smooth muscle tension depends on inner radius through a campanular relationship, which reflects the different overlapping of actin and myosin filaments. Active tension is therefore maximal at a particular optimal value of inner radius and then progressively decreases. We have

$$T_{m,j} = T_{max,j} \cdot \exp \left(- \left| \frac{r_j - r_{m,j}}{r_{t,j} - r_{m,j}} \right|^{n_{m,j}} \right) \quad j = 1, 2 \quad (11A)$$

where r_m represents the optimal radius at which smooth muscle exerts its maximal force, T_{max} is the corresponding active tension, and r_t and n_m are constant parameters used to

represent the appropriate shape of the campanular relationship.

For the sake of simplicity, we assumed that viscous stress (σ_v) has a linear dependency on the time derivative of wall strain. Thus

$$\sigma_{v,j} = \frac{\eta_j}{r_{0,j}} \left(\frac{dr_j}{dt} \right) \quad j = 1, 2 \quad (12A)$$

$$T_{v,j} = \sigma_{v,j} h_j \quad j = 1, 2 \quad (13A)$$

where η_j denotes wall viscosity.

An expression for wall thickness, to be used in Eq. 8A, has been computed by assuming that vessel wall volume remains constant. By neglecting longitudinal strain, we have

$$h_j = -r_j + \sqrt{r_j^2 + 2r_{0,j}h_{0,j} + h_{0,j}^2} \quad j = 1, 2 \quad (14A)$$

where h_0 is wall thickness in the unstressed condition (i.e., when $r = r_0$).

Equations 8A–14A provide a value for inner radius in the proximal and distal arterial segments if intravascular and extravascular pressures (P_j and P_{ic}) and the optimal smooth muscle tensions ($T_{max,j}$) are known. The latter parameter is under the control of regulatory actions (see *Cerebrovascular regulation mechanisms*). Starting with the radius, approximate expressions for intravascular conductance (G_j) and blood volume changes (dV_j/dt) for use in Eqs. 1A–3A, 6A, and 7A can be obtained by mimicking each segment as the parallel arrangement of several vessels with equal diameter. According to the Hagen-Poiseuille law, conductance is proportional to the fourth power of the inner radius

$$G_j = K_{C,j} r_j^4 \quad j = 1, 2 \quad (15A)$$

where K_C is a constant parameter whose value is set to obtain a physiological pressure drop in basal condition. Blood volume is, in turn, proportional to the second power of the inner radius

$$V_j = K_{V,j} r_j^2 \quad j = 1, 2 \quad (16A)$$

where a value for the constant parameter K_V is set to obtain physiological values of blood volume in each segment. By computing the time derivative of Eq. 16A, we obtain

$$\frac{dV_j}{dt} = 2K_{V,j} r_j \left(\frac{dr_j}{dt} \right) \quad j = 1, 2 \quad (17A)$$

Biomechanics of cerebral venous circulation. Because the intracranial venous circulation behaves in a passive way (4), we assumed that venous compliance is inversely proportional to transmural pressure. Hence, we have

$$C_{vi} = \frac{1}{k_{ven}(P_v - P_{ic} - P_{v1})} \quad (18A)$$

where k_{ven} and P_{v1} are constant parameters. The latter represents the transmural pressure value (usually slightly negative) at which cerebral veins collapse.

The conductance values for the intracranial veins (G_{pv} and G_{vs}) can be computed by assuming that the intracranial venous circulation behaves as a Starling resistor (50), i.e., the conductance of the terminal veins (G_{vs}) is supposed to depend on pressures through the following relationship

$$G_{vs} = G'_{vs} \left(\frac{P_v - P_{ic}}{P_v - P_{vs}} \right) \quad (19A)$$

where G'_{vs} is a constant parameter representing the value of conductance when $P_{ic} = P_{vs}$. Because of the collapse of the terminal vein, cerebral venous pressure is higher than ICP; hence, the large cerebral veins remain open. The conductance G_{pv} is independent of pressure; that is, a constant value for this parameter has been set throughout the present simulations.

Blood flow velocity in middle cerebral artery. The inner radius of the MCA (r_{MCA}) is computed as a function of transmural pressure, assuming a monoexponential pressure-radius relationship (20). The r_{MCA} is therefore a logarithmic function of transmural pressure, $P_a - P_{ic}$

$$r_{MCA} = r_{MCA n} \left[\frac{1}{K_{MCA}} \cdot \ln \left(\frac{P_a - P_{ic}}{P_{an} - P_{icn}} \right) + 1 \right] \quad (20A)$$

where K_{MCA} is a constant parameter and $r_{MCA n}$ denotes the inner radius in basal condition.

Finally, blood velocity (V_{MCA}) is computed as the ratio of blood flow and cross-sectional area, assuming that about one-third of total CBF passes through each MCA. Hence

$$V_{MCA} = \frac{q}{3} \left(\frac{1}{\pi r_{MCA}^2} \right) \quad (21A)$$

Cerebrovascular regulation mechanisms. Cerebrovascular control mechanisms affect smooth muscle tension in pial arteries by modifying the amplitude of the active tension relationship (i.e., T_{max} in Eq. 11A). We have

$$T_{max,j} = T_{max0,j} (1 + M_j) \quad j = 1, 2 \quad (22A)$$

where T_{max0} is the optimal smooth muscle tension in basal condition and M is an activation factor that accounts for the degree of smooth muscle contraction or dilation. In basal conditions $M = 0$. Furthermore, $-1 < M < 0$ indicates vasodilation, whereas $0 < M < 1$ represents vasoconstriction.

The activation factor is the result of two contributions, x_{aut} and x_{CO_2} , which account for the effect of autoregulation and CO₂ reactivity, respectively. Both are state variables, the dynamics of which have been assumed to be of the first order (see below).

CEREBRAL AUTOREGULATION. In accordance with physiological literature, we assumed that autoregulation acts on large pial arteries and pial arterioles through two distinct feedback mechanisms. Smooth muscle tension in the proximal segment depends on perfusion pressure changes. Hence, the following differential equation holds for the variable $x_{aut,1}$

$$\tau_{aut,1} \left(\frac{dx_{aut,1}}{dt} \right) = -x_{aut,1} + G_{aut,1} (P_a - P_v - P_{an} + P_{vn}) \quad (23A)$$

where $G_{aut,1}$ and $\tau_{aut,1}$ are the mechanism gain and time constant and $P_{an} - P_{vn}$ is normal CPP. According to Eq. 23A, any decrease in CPP causes a vasodilation in large pial arteries, whereas a perfusion pressure increase causes vasoconstriction.

In the small pial arteries (second segment in Fig. 1), we assumed that autoregulation is triggered by changes in CBF. Accordingly, the quantity $x_{aut,2}$ is governed by the following differential equation

$$\tau_{aut,2} \left(\frac{dx_{aut,2}}{dt} \right) = -x_{aut,2} + G_{aut,2} \left(\frac{q - q_n}{q_n} \right) \quad (24A)$$

where, as in Eq. 23A, $G_{aut,2}$ and $\tau_{aut,2}$ are gain and time constants, and the parameter q_n represents the value of CBF that satisfies the metabolic need (and so does not activate the

autoregulatory action). Equation 24A implies that a decrease in CBF below q_n causes vasodilation in small pial arteries, whereas the opposite effect is produced by an increase in CBF.

CO₂ REACTIVITY. Because CO₂ acts mainly through changes in the pH of the perivascular space, we assumed that the state variables $x_{CO_2,j}$ ($j = 1, 2$) depend on the logarithm of CO₂ pressure in arterial blood. Moreover, the nature of CO₂ reactivity does not differ substantially in large and small pial arteries. The following differential equations can thus be written

$$\tau_{CO_2,j} \left(\frac{dx_{CO_2,j}}{dt} \right) = -x_{CO_2,j} - G_{CO_2,j} A_{CO_2} \cdot \log_{10} \left(\frac{Pa_{CO_2}}{Pa_{CO_2,n}} \right) \quad (25A)$$

$j = 1, 2$

where G_{CO_2} and τ_{CO_2} denote the mechanism gain and time constant and the subscript n is used to represent the Pa_{CO_2} value that does not affect the basal smooth muscle tension. According to Eq. 25A, hypercapnia causes vasodilation in both pial segments, whereas hypocapnia causes vasoconstriction. Finally, in accordance with the corrective factor A_{CO_2} , we assumed that the strength of the CO₂ regulation mechanism remains quite constant when CBF is normal or moderately decreased but rapidly drops to zero during severe ischemia. We used the following dependence of A_{CO_2} on CBF

$$A_{CO_2} = \frac{1}{1 + \exp[-K_{CO_2}(q - q_n)/q_n - b_{CO_2}]} \quad j=1, 2 \quad (26A)$$

where K_{CO_2} and b_{CO_2} are constant parameters. These parameters were set so that A_{CO_2} remains almost 1 until CBF is greater than 50% of q_n and then exponentially decreases (see inset in Fig. 4). As a consequence, the CO₂ reactivity of pial vessels vanishes during severe ischemia.

INTERACTION BETWEEN AUTOREGULATION AND CO₂ REACTIVITY. The two state variables x_{aut} and x_{CO_2} interact in a nonlinear way through a sigmoidal relationship, yielding the activation factor M . We therefore have

$$M_j = \frac{M_{min,j} + M_{max,j} \exp[(x_{aut,j} + x_{CO_2,j})/K_{M,j}]}{1 + \exp[(x_{aut,j} + x_{CO_2,j})/K_{M,j}]} \quad (27A)$$

$j = 1, 2$

where M_{min} and M_{max} are the lower and upper saturation levels of the sigmoidal relationship, representing the limits for smooth muscle tension, and K_M is a constant parameter that permits setting of the central slope (i.e., the slope when $x_{aut} + x_{CO_2} = 0$). In this model we assumed that the central slope is always equal to 1. This is achieved by assuming $K_{M,j} = (M_{max,j} - M_{min,j})/4$. Because of this assumption, the gain of each mechanism acting individually is equal to G_{aut} and G_{CO_2} in Eqs. 23A–25A.

Address for reprint requests: M. Ursino, Dipartimento di Elettronica, Informatica e Sistemistica, viale Risorgimento 2, I-40136 Bologna, Italy.

Received 31 July 1997; accepted in final form 28 January 1998.

REFERENCES

- Aaslid, R., T.-M. Markwalder, and H. Nornes. Noninvasive transcranial Doppler ultrasound recording of flow velocity in basal cerebral arteries. *J. Neurosurg.* 57: 769–774, 1982.
- Artru, A. A., and P. S. Colley. Cerebral blood flow responses to hypocapnia during hypotension. *Stroke* 15: 878–883, 1984.
- Auer, L. M. Pial arterial reactions to hyper- and hypocapnia: a dynamic experimental study in cats. *Eur. Neurol.* 17: 351–362, 1978.
- Auer, L. M., N. Ishiyama, and R. Pucher. Cerebrovascular response to intracranial hypertension. *Acta Neurochir. (Wien)* 84: 124–128, 1987.
- Avezaat, C. J. J., J. H. M. van Eijndhoven, and D. J. Wyper. Cerebrospinal fluid pulse pressure and intracranial volume-pressure relationship. *J. Neurol. Neurosurg. Psychiatry* 42: 687–700, 1979.
- Baumbach, G. L., and D. D. Heistad. Regional, segmental, and temporal heterogeneity of cerebral vascular autoregulation. *Ann. Biomed. Eng.* 13: 303–310, 1985.
- Charlton, J. D., H. A. Guess, J. D. Mann, H. T. Nagle, and R. N. Johnson. A pressure controller for estimating parameters for a nonlinear CSF model. *IEEE Trans. Biomed. Eng.* 35: 752–754, 1988.
- Cold, G. E. Measurements of CO₂ reactivity and barbiturate reactivity in patients with severe head injury. *Acta Neurochir. (Wien)* 98: 153–163, 1989.
- D'Alecy, L. G., C. J. Rose, and S. A. Sellers. Sympathetic modulation of hypercapnic cerebral vasodilation in dogs. *Circ. Res.* 45: 771–785, 1979.
- Davis, M. J., and R. W. Gore. Length-tension relationship of vascular smooth muscle in single arterioles. *Am. J. Physiol.* 256 (*Heart Circ. Physiol.* 25): H630–H640, 1989.
- Ekström-Jodal, B., E. Häggendal, L.-E. Linder, and N. J. Nilsson. Cerebral blood flow autoregulation at high arterial pressures and different levels of carbon dioxide tension in dogs. *Eur. Neurol.* 6: 6–10, 1971.
- Enevoldsen, E. M., and F. T. Jensen. Autoregulation and CO₂ responses of cerebral blood flow in patients with acute severe head injury. *J. Neurosurg.* 48: 689–703, 1978.
- Giller, C. A., G. Bowman, H. Dyer, L. Mootz, and W. Krippner. Cerebral arterial diameters during changes in blood pressure and carbon dioxide during craniotomy. *Neurosurgery* 32: 737–742, 1993.
- Giulioni, M., and M. Ursino. Impact of cerebral perfusion pressure and autoregulation on intracranial dynamics: a modeling study. *Neurosurgery* 39: 1005–1015, 1996.
- Göbel, U., B. Klein, H. Schröck, and W. Kuschinsky. Lack of capillary recruitment in the brains of awake rats during hypercapnia. *J. Cereb. Blood Flow Metab.* 9: 491–499, 1989.
- Häggendal, E., and B. Johansson. Effects of arterial carbon dioxide tension and oxygen saturation on cerebral blood flow autoregulation in dogs. *Acta Physiol. Scand.* 66, Suppl. 258: 27–53, 1965.
- Harper, A. M. Autoregulation of cerebral blood flow: influence of the arterial blood pressure on the blood flow through the cerebral cortex. *J. Neurol. Neurosurg. Psychiatry* 29: 398–403, 1966.
- Harper, A. M., and H. I. Glass. Effect of alterations in the arterial carbon dioxide tension on the blood flow through the cerebral cortex at normal and low arterial blood pressure. *J. Neurol. Neurosurg. Psychiatry* 28: 449–452, 1965.
- Harper, S. L., H. G. Bohlen, and M. J. Rubin. Arterial and microvascular contributions to cerebral cortical autoregulation in rats. *Am. J. Physiol.* 246 (*Heart Circ. Physiol.* 15): H17–H24, 1984.
- Hayashi, K., H. Handa, S. Nagasawa, A. Okumura, and K. Moritake. Stiffness and elastic behavior of human intracranial and extracranial arteries. *J. Biomech.* 13: 175–184, 1979.
- Hillen, B., B. A. H. Drinkenburg, H. W. Hoogstraten, and L. Post. Analysis of flow and vascular resistance in a model of the circle of Willis. *J. Biomech.* 21: 807–814, 1988.
- Hoffman, H. Biomathematics of intracranial CSF and hemodynamics, simulation and analysis with the aid of a mathematical model. *Acta Neurochir. Suppl. (Wien)* 40: 117–130, 1987.
- Jones, S. C., B. Bose, A. J. Furlan, H. T. Friel, K. A. Easley, M. P. Meredith, and J. R. Little. CO₂ reactivity and heterogeneity of cerebral blood flow in ischemic, border zone, and normal cortex. *Am. J. Physiol.* 257 (*Heart Circ. Physiol.* 26): H473–H482, 1989.
- Kontos, H. A., A. J. Raper, and J. L. Patterson, Jr. Analysis of vasoactivity of local pH, PCO₂, and bicarbonate on pial vessels. *Stroke* 8: 358–360, 1977.

25. **Kontos, H. A., E. P. Wei, R. M. Navari, J. E. Levasseur, W. I. Rosenblum, and J. L. Patterson, Jr.** Responses of cerebral arteries and arterioles to acute hypotension and hypertension. *Am. J. Physiol.* 234 (*Heart Circ. Physiol.* 3): H371–H383, 1978.
26. **Levasseur, J. E., and H. A. Kontos.** Effects of anesthesia on cerebral arteriolar responses to hypercapnia. *Am. J. Physiol.* 257 (*Heart Circ. Physiol.* 26): H85–H88, 1989.
27. **Lodi, C. A., A. Ter Minassian, L. Beydon, and M. Ursino.** Modeling cerebral autoregulation and CO₂ reactivity in patients with severe head injury. *Am. J. Physiol.* 274 (*Heart Circ. Physiol.* 43): H1729–H1741, 1998.
28. **Lundberg, N.** Continuous recording and control of ventricular fluid pressure in neurosurgical practice. *Acta Psychiatr. Scand.* 36: 1–193, 1960.
29. **MacKenzie, E. T., J. K. Farrar, W. Fitch, D. I. Graham, P. C. Gregory, and A. M. Harper.** Effects of hemorrhagic hypotension on the cerebral circulation. I. Cerebral blood flow and pial arteriolar caliber. *Stroke* 10: 711–718, 1979.
30. **Markwalder, T.-M., P. Grolimund, R. W. Seiler, F. Roth, and R. Aaslid.** Dependency of blood flow velocity in the middle cerebral artery on end-tidal carbon dioxide partial pressure: a transcranial ultrasound Doppler study. *J. Cereb. Blood Flow Metab.* 4: 368–372, 1984.
31. **Marmarou, A., K. Shulman, and J. LaMorgese.** Compartmental analysis of compliance and outflow resistance of the cerebrospinal fluid system. *J. Neurosurg.* 43: 523–534, 1975.
32. **Mchedlishvili, G.** *Arterial Behavior and Blood Circulation in the Brain.* New York: Plenum, 1986.
33. **Milnor, W. R.** *Hemodynamics.* Baltimore, MD: Williams and Wilkins, 1982.
34. **Muizelaar, J. P., H. G. Van Der Poel, Z. Li, H. A. Kontos, and J. E. Levasseur.** Pial arteriolar vessel diameter and CO₂ reactivity during prolonged hyperventilation in the rabbit. *J. Neurosurg.* 69: 923–927, 1988.
35. **Nelson, R. J., M. Czosnyka, J. D. Pickard, W. Maksymowicz, S. Perry, J. L. Martin, and A. H. J. Lovick.** Experimental aspects of cerebrospinal hemodynamics: the relationship between blood flow velocity waveform and cerebral autoregulation. *Neurosurgery* 31: 705–710, 1992.
36. **Newell, D. W., R. Aaslid, A. Lam, T. S. Mayberg, and R. Winn.** Comparison of flow and velocity during autoregulation testing in humans. *Stroke* 25: 793–797, 1994.
37. **Paulson, O. B., J. Olesen, and M. S. Christensen.** Restoration of autoregulation of cerebral blood flow by hypocapnia. *Neurology* 22: 286–293, 1972.
38. **Paulson, O. B., S. Strandgaard, and L. Edvinsson.** Cerebral autoregulation. *Cerebrovasc. Brain Metab. Rev.* 2: 161–192, 1990.
39. **Raichle, M. E., and H. L. Stone.** Cerebral blood flow autoregulation and graded hypercapnia. *Eur. Neurol.* 6: 1–5, 1971.
40. **Raper, A. J., H. A. Kontos, and J. L. Patterson, Jr.** Response of pial precapillary vessels to changes in arterial carbon dioxide tension. *Circ. Res.* 28: 518–523, 1971.
41. **Reivich, M.** Arterial PCO₂ and cerebral hemodynamics. *Am. J. Physiol.* 206: 25–35, 1964.
42. **Rosner, M. J., and D. P. Becker.** Cerebral perfusion pressure: link between intracranial pressure and systemic circulation. In: *Cerebral Blood Flow: Physiological and Clinical Aspects*, edited by J. H. Wood. New York: McGraw-Hill, 1987, p. 425–448.
43. **Schneider, W., M. Wahl, W. Kuschinsky, and K. Thurau.** The use of microelectrodes for measurements of local H⁺ activity in the cortical subarachnoidal space of cats. *Pflügers Arch.* 372: 103–107, 1977.
44. **Seiler, R. W., and A. C. Nirkko.** Effect of nimodipine on cerebrovascular response to CO₂ in asymptomatic individuals and patients with subarachnoid hemorrhage: a transcranial Doppler ultrasound study. *Neurosurgery* 27: 247–251, 1990.
45. **Severinghaus, J. W., and N. Lassen.** Step hypocapnia to separate arterial from tissue PCO₂ in the regulation of cerebral blood flow. *Circ. Res.* 20: 272–278, 1967.
46. **Shalit, M. N., O. M. Reinmuth, S. Shimojyo, and P. Scheinberg.** Carbon dioxide and cerebral circulatory control. III. The effects of brain stem lesions. *Arch. Neurol.* 17: 342–353, 1967.
47. **Sorek, S., J. Bear, and Z. Karni.** Resistances and compliances of a compartmental model of the cerebrovascular system. *Ann. Biomed. Eng.* 17: 1–12, 1989.
48. **Tenjin, H., T. Yamaki, Y. Nakagawa, T. Kuboyama, T. Ebisu, N. Kobori, S. Ueda, and N. Mizukawa.** Impairment of CO₂ reactivity in severe head injury patients: an investigation using thermal diffusion method. *Acta Neurochir. (Wien)* 104: 121–125, 1990.
49. **Ursino, M.** A mathematical model of overall cerebral blood flow regulation in the rat. *IEEE Trans. Biomed. Eng.* 38: 795–807, 1991.
50. **Ursino, M.** A mathematical study of human intracranial hydrodynamics. I. The cerebrospinal fluid pulse pressure. *Ann. Biomed. Eng.* 16: 379–402, 1988.
51. **Ursino, M., and P. Di Giammarco.** A mathematical model of the relationship between cerebral blood volume and intracranial pressure changes: the generation of plateau waves. *Ann. Biomed. Eng.* 19: 15–42, 1991.
52. **Ursino, M., M. Iezzi, and N. Stocchetti.** Intracranial pressure dynamics in patients with acute brain damage: a critical analysis with the aid of a mathematical model. *IEEE Trans. Biomed. Eng.* 42: 529–540, 1995.
53. **Wei, E. P., H. A. Kontos, and J. L. Patterson, Jr.** Dependence of pial arteriolar response to hypercapnia on vessel size. *Am. J. Physiol.* 238 (*Heart Circ. Physiol.* 7): H697–H703, 1980.